





Cite this: DOI: 10.1039/d6cc01957a

 Received 31st March 2026,
 Accepted 6th June 2026

DOI: 10.1039/d6cc01957a

rsc.li/chemcomm

Chirality transfer to achiral strands and helicity control through selective heteroleptic assembly of double-helical monometallofoldamers

 Kotaro Matsumura, Shinji Murayama, Yoshitaka Tsuchido  and
 Hidetoshi Kawai *

Highly selective construction of heteroleptic double helices was achieved by utilizing bulky substituents to destabilize homoleptic complexation. This strategic design enables efficient chirality transfer to an achiral strand and solvent-dependent helicity inversion, achieving a twofold amplification of the total chiroptical output that far surpasses our previous system.

In biological systems, DNA and RNA serve as the quintessential platforms for the storage, replication, and transcription of genetic information through double-helical frameworks mediated by complementary hydrogen bonding. To artificially emulate these sophisticated processes, the construction of hetero-double helices—where two distinct strands selectively self-assemble (social self-sorting) over their homoleptic counterparts (narcissistic self-sorting)—is essential (Fig. 1a).^{1–13} Within such hetero-double helices, structural information and functionality can be transmitted from a “template” strand to a “partner” strand (Fig. 1b). While chiral information transfer from a chiral template strand to an achiral strand has been demonstrated in several limited examples,^{9–11} the general application of these systems is often hampered by the lack of high-fidelity social self-sorting. Constructing structurally controllable heteroleptic complexes remains a significant challenge, as many systems favor homoleptic assembly or result in statistical mixtures unless specific complementary interactions are employed.

The helicity inversion switching in response to achiral stimuli is attractive for the reversible control of chirality.^{14–17} To date, various external stimuli—solvents,^{3,18–21} guests or ions,^{22–24} and light^{25,26}—have been employed for helix inversions in polymers and supramolecular assemblies. In achiral-chiral hetero-double helices, the helicity of the achiral strand is synchronized with that of the chiral strand through cooperative inter-strand communication. This synchronization potentially allows for the precise chirality transfer and even the cooperative

switching of the entire helical framework. However, achieving such dynamic behavior specifically in heteroleptic systems remains difficult due to a “trade-off” between structural rigidity and flexibility: many double-helical complexes lack the conformational freedom necessary for stimuli responsive inversion due to the rigid nature of their bridging coordination bonds.

We have previously developed double-helical monometallofoldamers $[M(\mathbf{1}_2)]^{n+}$ (Zn(II), Cu(II), Cu(I), Ag(I)) constructed from short-stranded foldamers^{27–31} incorporating two L-shaped dibenzopyrrolo[1,2-*a*][1,8]naphthyridine units^{32,33} by a bipyridine unit.^{29,31} These complexes exhibit dynamic structural switching between double-helical and open forms, including *M/P* helicity inversion driven by solvent polarity.^{29,31} While we successfully constructed a heteroleptic complex $[Zn(\mathbf{1a})(\mathbf{1b})][OTf]_2$ using an achiral strand $\mathbf{1a}$ and a chiral strand $\mathbf{1b}$, its formation as a statistical mixture limited the efficiency of chiral amplification.²⁹ Consequently, a novel design is required to achieve selective social

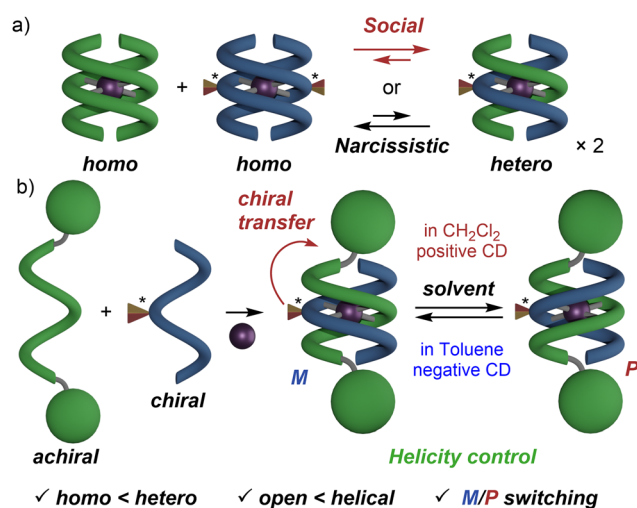


Fig. 1 (a) Equilibrium between homoleptic- and heteroleptic-double helices. (b) Strategy for steric-driven selective heteroleptic complexation, achieving chirality transfer and helicity control.

Department of Chemistry, Faculty of Science, Tokyo University of Science, 1–3 Kagurazaka, Shinjuku-ku, Tokyo 162–8601, Japan. E-mail: kawaih@rs.tus.ac.jp



self-sorting while maintaining a dynamic helical framework capable of helicity inversion. Herein, we report the highly selective construction of a heteroleptic double-helix $[\text{Ag}(\mathbf{1})(\mathbf{2a})][\text{OTf}]$ designed for efficient chirality transfer and helicity control (Fig. 1b, 2). By incorporating bulky tris(biphenyl)methoxy groups at the termini of strand $\mathbf{2a}$, we successfully destabilized narcissistic homoleptic complexation, driving social self-assembly with high selectivity. This selective formation enables a twofold amplification of the Cotton effect, effectively enhancing the chiroptical output of the chiral template within the heteroleptic framework. Furthermore, the achiral strand exhibits helicity inversion dictated by the chiral strand in response to solvent stimuli, demonstrating the potential of heteroleptic double helices for the controlled transfer and stimuli-responsive switching of chiral information.

To drive social self-sorting, we designed strand $\mathbf{2a}$ bearing bulky tris(biphenyl)methoxy groups at both termini to sterically destabilize narcissistic homoleptic complexation (Fig. 2a). Strand $\mathbf{2a}$ was synthesized *via* Suzuki–Miyaura coupling and subsequent etherification (for details, see Scheme S1 in SI).

The complexation behaviors of the strands $\mathbf{1a}$, $\mathbf{1b}$ and $\mathbf{2a}$ were evaluated by ^1H NMR spectroscopy (Fig. S4–S6 and 2b–d). Initially, the homoleptic complex $[\text{Ag}(\mathbf{2a})_2][\text{OTf}]$ was prepared by complexing strand $\mathbf{2a}$ with $\text{Ag}(\text{I})$ (Fig. 2d, Fig. S4 and Scheme S7 in SI). The resulting species exhibited complicated ^1H NMR signals, reflecting a loss of symmetry compared to the previously reported homoleptic double-helical complexes derived from strand $\mathbf{1a}$ and $\mathbf{1b}$.^{29,31} This suggested that strand $\mathbf{2a}$ was unable to form a highly symmetric double-helical structure due to the steric bulk of the substituents, leading to a distribution of diverse conformations, such as open forms. This was further supported by the absence of a characteristic hypochromic effect in the UV-vis spectra (Fig. S17 and S28 in SI).

In contrast, mixing achiral strands $\mathbf{1a}$, $\mathbf{2a}$ and AgOTf in $\text{CHCl}_3/\text{CH}_3\text{CN}$ (19:1) led to the highly selective formation of the heteroleptic double-helical complex $[\text{Ag}(\mathbf{1a})(\mathbf{2a})][\text{OTf}]$ (Fig. 2a and Scheme S8). The ^1H NMR spectrum revealed a predominant species distinct from either homoleptic complex, with an estimated ratio of 1:10:1 for $[\text{Ag}(\mathbf{1a})_2][\text{OTf}]/[\text{Ag}(\mathbf{1a})(\mathbf{2a})][\text{OTf}]/[\text{Ag}(\mathbf{2a})_2][\text{OTf}]$ (Fig. S5b in SI). The characteristic upfield shifts of bipyridine protons H_a and H_b (5.57–6.56 ppm) and ROESY correlations ($\text{A}_{1a}\text{--}\text{A}_{2a}$, $\text{A}_{1a}\text{--}\text{L}_{2a}$, $\text{L}_{1a}\text{--}\text{A}_{2a}$, $\text{L}_{1a}\text{--}\text{L}_{2a}$, Fig. S16 in SI) confirmed the double-helical structure.^{29,31} These results indicate that the bulky substituents not only destabilize $[\text{Ag}(\mathbf{2a})_2][\text{OTf}]$ but also relatively stabilize the double-helical framework of heteroleptic $[\text{Ag}(\mathbf{1a})(\mathbf{2a})][\text{OTf}]$ over homoleptic $[\text{Ag}(\mathbf{1a})_2][\text{OTf}]$, which exists primarily in open forms (double-helical form/open form ratio $\sim 7:93$) in CDCl_3 at 298 K.³¹ Importantly, in contrast to the kinetically inert $\text{Zn}(\text{II})$ system which required kinetic preparation by mixing the ligands prior to metal addition,²⁹ the labile nature of $\text{Ag}(\text{I})$ ions allows the system to reach a thermodynamic equilibrium, wherein the heteroleptic complex is favored as the thermodynamically most stable species.

Encouraged by this high selectivity, we prepared the chiral heteroleptic complex $[\text{Ag}(\mathbf{1b})(\mathbf{2a})][\text{OTf}]$ using the chiral strand $\mathbf{1b}$ (Fig. 2a, c). The ^1H NMR spectrum clearly demonstrates the selective formation of the heteroleptic complex. While the homoleptic complex $[\text{Ag}(\mathbf{1b})_2][\text{OTf}]$ exhibited peaks corresponding to both double-helical and open forms (Fig. 2b, helical/open = 1:3), the heteroleptic $[\text{Ag}(\mathbf{1b})(\mathbf{2a})][\text{OTf}]$ showed only two sets of characteristics of the double-helical form, which suggested the formation of a highly stable double-helical structure. These peaks are attributed to the diastereomers $[(P)\text{--}(R)\text{--}]$ and $[(M)\text{--}(R)\text{--}]\text{Ag}(\mathbf{1b})(\mathbf{2a})][\text{OTf}]$, revealing a clear helicity bias with an intensity

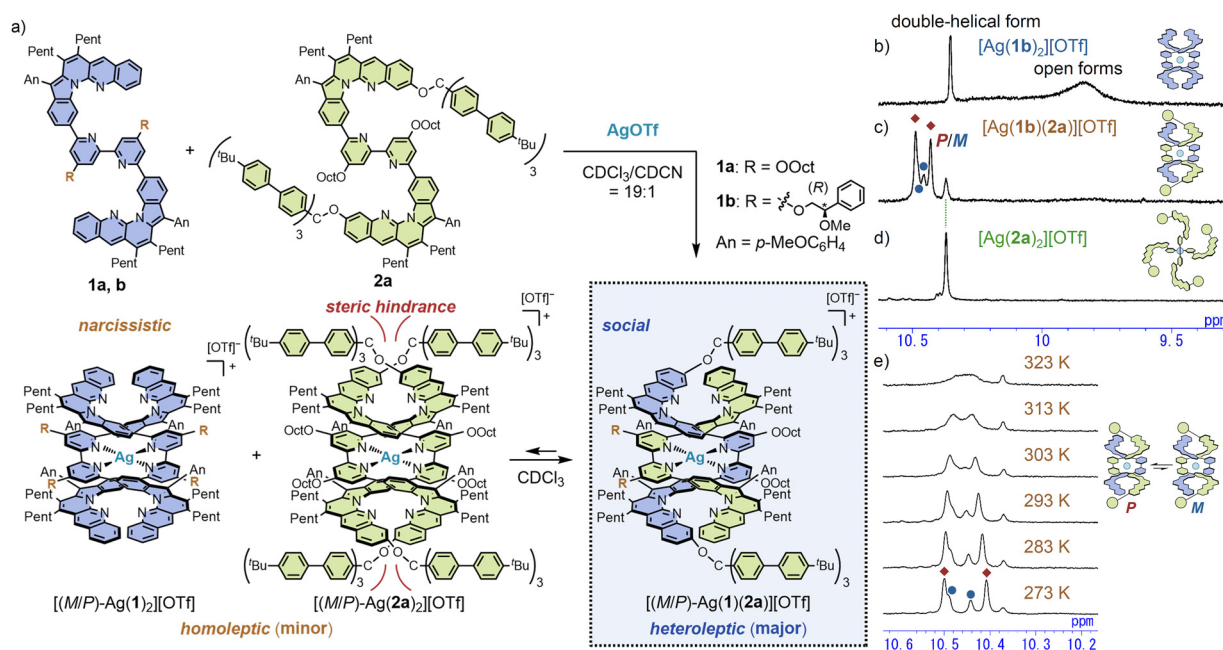


Fig. 2 (a) Highly selective complexation to heteroleptic double-helical monometallofoldamers $[\text{Ag}(\mathbf{1})(\mathbf{2a})][\text{OTf}]$. ^1H NMR spectra (9.2–11.0 ppm, CDCl_3 , 298 K) of (b) $[\text{Ag}(\mathbf{1b})_2][\text{OTf}]$ ($[\mathbf{1b}] = 2.0$ mM), (c) a mixture of $\mathbf{1b}$, $\mathbf{2a}$, and AgOTf ($[\mathbf{1b}] = 1.0$ mM, $[\mathbf{2a}] = 1.0$ mM), and (d) $[\text{Ag}(\mathbf{2a})_2][\text{OTf}]$ ($[\mathbf{2a}] = 2.0$ mM). (e) VT-NMR spectra of $[\text{Ag}(\mathbf{1b})(\mathbf{2a})][\text{OTf}]$ (10.2–10.6 ppm, CDCl_3 , 273–323 K).



ratio of $\sim 3:1$ in favor of the (*P*)-helix as assigned by the positive CD sign and a related TD-DFT calculation,³¹ achieved even in a heteroleptic system bearing only two chiral auxiliaries. Furthermore, the predominance of $[\text{Ag}(\mathbf{1b})(\mathbf{2a})][\text{OTf}]$ ($[\text{Ag}(\mathbf{1b})_2]/[\text{Ag}(\mathbf{1b})(\mathbf{2a})]/[\text{Ag}(\mathbf{2a})_2] = 1:10:1$) remained consistent in toluene- d_8 and CD_2Cl_2 , indicating that the equilibrium among the homoleptic and heteroleptic complexes is not significantly solvent-dependent (Fig. S7 and S8 in SI). To investigate the thermodynamic properties and dynamic nature of this helicity bias, variable-temperature NMR measurements were performed (Fig. 2e). Upon heating from 273 K to 323 K, the peaks for the *P*- and *M*-isomers coalesced, accompanied by a decrease in the helicity bias (from $\sim 3:1$ at 273 K to $\sim 2:1$ at 293 K). This temperature dependence demonstrates that the helicity preference is enthalpy-driven. Remarkably, while the homoleptic $[\text{Ag}(\mathbf{1b})_2][\text{OTf}]$ showed coalesced signals even at 298 K (Fig. 2b), the coalescence observed at 323 K in the heteroleptic $[\text{Ag}(\mathbf{1b})(\mathbf{2a})][\text{OTf}]$ reveals that the bulky groups not only maintain the highly efficient heteroleptic assembly but also successfully increase the activation barrier for the helicity inversion.

The high-fidelity transfer of chiral information from $\mathbf{1b}$ to $\mathbf{2a}$ was evidenced by CD measurements of the resulting heteroleptic complex $[\text{Ag}(\mathbf{1b})(\mathbf{2a})][\text{OTf}]$ (Fig. 3 and 4a).³⁴ Notably, $[\text{Ag}(\mathbf{1b})(\mathbf{2a})][\text{OTf}]$ exhibited a positive Cotton effect in CH_2Cl_2 (as well as in CHCl_3 , MeOH, *i*-PrOH and THF), which inverted to a strong negative Cotton effect in toluene.³⁵ This solvent-dependent helicity inversion is consistent with the behavior of the homoleptic analogue $[\text{Ag}(\mathbf{1b})_2][\text{OTf}]$ (Fig. 3a),³⁶ indicating that the chiral and achiral strands function cooperatively throughout the double-helical framework. Such inter-strand communication not only allows the chiral strand $\mathbf{1b}$ to induce a specific helicity in the achiral strand $\mathbf{2a}$ but also facilitates the helicity inversion of the entire heteroleptic assembly, driven by the stimuli-responsive switching of the chiral strand.

The high selectivity of this heteroleptic assembly provides a molecular basis for artificial information transfer, reminiscent of biological systems. Notably, the chiroptical properties and solvent-dependent helicity inversion of the heteroleptic $[\text{Ag}(\mathbf{1b})(\mathbf{2a})][\text{OTf}]$ remarkably mirror those of the homoleptic template $[\text{Ag}(\mathbf{1b})_2][\text{OTf}]$. This suggests that both the chiral information and the dynamic switching characteristics of a single strand $\mathbf{1b}$ could be effectively transferred through the co-assembly with achiral strands $\mathbf{2a}$ into the double-helical framework (Fig. 1b). As illustrated in Fig. 3b, if the chiral template $\mathbf{1b}$, which originally forms a single homo-double helix $[\text{Ag}(\mathbf{1b})_2][\text{OTf}]$ (Fig. 3a), were to selectively assemble with two achiral strands $\mathbf{2a}$, two sets of heteroleptic $[\text{Ag}(\mathbf{1b})(\mathbf{2a})][\text{OTf}]$ would be produced. Consequently, this chiral information transfer process would lead to a twofold amplification of the total chiroptical output, effectively doubling the chiral signature of the system.

To verify the chiral amplification derived from this selective assembly mechanism, we compared the CD intensities of the heteroleptic $[\text{Ag}(\mathbf{1b})(\mathbf{2a})][\text{OTf}]$ and the homoleptic $[\text{Ag}(\mathbf{1b})_2][\text{OTf}]$ (Fig. 4b). Remarkably, the addition of one equivalent of achiral strand $\mathbf{2a}$ to a mixture of chiral strand $\mathbf{1b}$ and AgOTf resulted in a Cotton effect amplified by 2.3-fold in toluene and 2.5-fold in

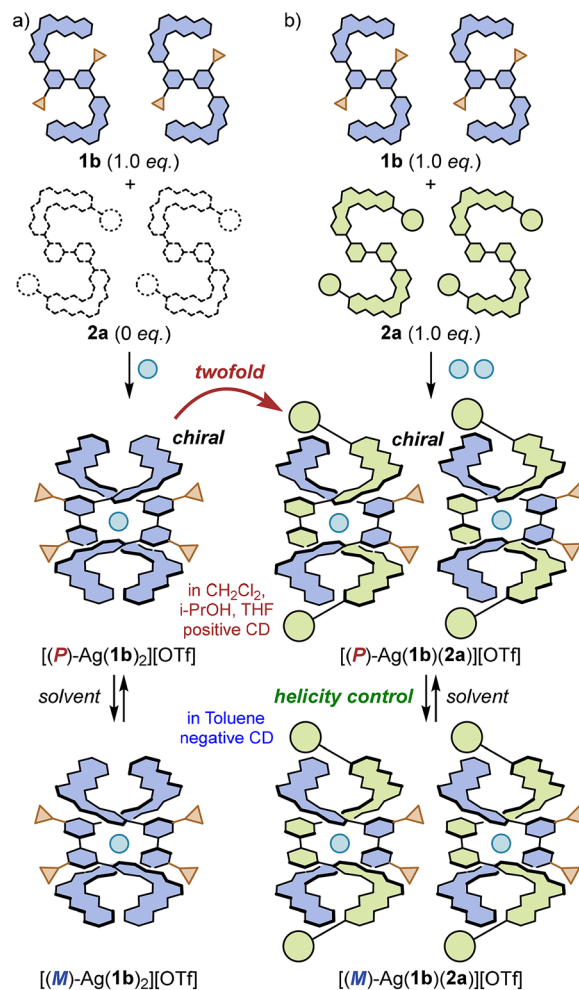


Fig. 3 The complexation of (a) $\mathbf{1b}$ (1.0 equiv.) with AgOTf (0.50 equiv.); (b) $\mathbf{1b}$ (1.0 equiv.) and $\mathbf{2a}$ (1.0 equiv.) with AgOTf (1.0 equiv.) and solvent-dependent helicity switching in $[\text{Ag}(\mathbf{1b})_2][\text{OTf}]$ and $[\text{Ag}(\mathbf{1b})(\mathbf{2a})][\text{OTf}]$.

CH_2Cl_2 compared to the system containing only $\mathbf{1b}$ and AgOTf.³⁵ These amplification factors are significantly higher than the 1.1–1.2-fold increase previously reported for the Zn(II) system,²⁹ where the formation of a statistical mixture limited the efficiency. This significant enhancement clearly originates from the highly efficient heteroleptic distribution of chiral information from a single chiral entity, $[\text{Ag}(\mathbf{1b})_2][\text{OTf}]$, into two heteroleptic $[\text{Ag}(\mathbf{1b})(\mathbf{2a})][\text{OTf}]$, which retain the same chiroptical characteristics. Furthermore, by combining the achiral strand $\mathbf{2a}$ with the stimuli-responsive template $\mathbf{1b}$, we have realized a system that enables the simultaneous amplification and inversion of chiroptical signals. This dual functionality provides critical insights for the design of sophisticated supramolecular systems with advanced functions in information transfer.

In summary, we have demonstrated the highly selective construction of heteroleptic double helices $[\text{Ag}(\mathbf{1})(\mathbf{2a})][\text{OTf}]$ through the social self-sorting of AgOTf with strands $\mathbf{1}$ and $\mathbf{2a}$, thanks to the thermodynamic control enabled by the Ag(I) ions. The strategic introduction of bulky groups in $\mathbf{2a}$ effectively destabilizes narcissistic homoleptic assembly. Furthermore, an



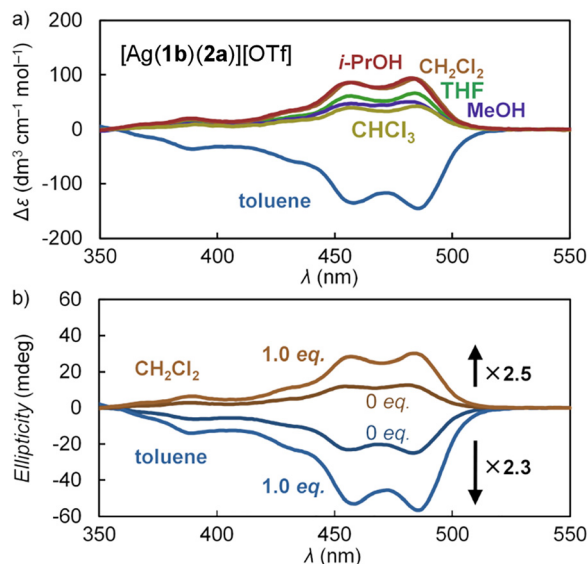


Fig. 4 (a) CD spectra of $[\text{Ag}(\mathbf{1b})(\mathbf{2a})][\text{OTf}]$ in *i*-PrOH (red), CH_2Cl_2 (brown), CHCl_3 (yellow), THF (green), toluene (blue) and MeOH (purple) (r.t., $[\text{Ag}(\mathbf{1b})(\mathbf{2a})][\text{OTf}] = 5.0 \mu\text{M}$). (b) CD spectra in the presence of 0 and 1.0 equiv. of $\mathbf{2a}$ in CH_2Cl_2 (brown) and in toluene (blue) (r.t., $[\mathbf{1b}] = 10 \mu\text{M}$).

increased activation barrier for the dynamic process effectively stabilizes the double helix, suppressing the competitive open-form dissociation. Notably, the chiral heteroleptic $[\text{Ag}(\mathbf{1b})(\mathbf{2a})][\text{OTf}]$ exhibited both an amplified Cotton effect mediated by high-fidelity chiral transfer through the rigid L-shaped double-helical framework and solvent-induced helicity switching. This dual functionality of chiroptical amplification and helicity inversion, enabled by the efficient heteroleptic distribution from homoleptic precursors to hetero-double helices, provides a novel molecular design guideline for the precise transfer and regulation of chiral information in artificial supramolecular systems.

Conflicts of interest

There are no conflicts to declare.

Data availability

The supporting data has been provided as part of the supplementary information (SI). Supplementary information: Fig. S1–S41; Schemes S1–S11; Tables S1, S2; NMR spectra; UV-vis and CD spectra; X-ray crystallography data; and further experimental details, See DOI: <https://doi.org/10.1039/d6cc01957a>.

CCDC 2534923 and 2534924 contain the supplementary crystallographic data for this paper.^{37a,b}

References

- B. Hasenknopf, J. M. Lehn, G. Baum and D. Fenske, *Proc. Natl. Acad. Sci. U. S. A.*, 1996, **93**, 1397–1400.
- Y. Tanaka, H. Katagiri, Y. Furusho and E. Yashima, *Angew. Chem., Int. Ed.*, 2005, **44**, 3867–3870.
- T. Hasegawa, Y. Furusho, H. Katagiri and E. Yashima, *Angew. Chem., Int. Ed.*, 2007, **46**, 5885–5888.
- H. Ito, M. Ikeda, T. Hasegawa, Y. Furusho and E. Yashima, *J. Am. Chem. Soc.*, 2011, **133**, 3419–3432.
- C. Zhan, J.-M. Léger and I. Huc, *Angew. Chem., Int. Ed.*, 2006, **45**, 4625–4628.
- M. L. Singleton, G. Pirotte, B. Kauffmann, Y. Ferrand and I. Huc, *Angew. Chem., Int. Ed.*, 2014, **53**, 13140–13144.
- R. Amemiya, N. Saito and M. Yamaguchi, *J. Org. Chem.*, 2008, **73**, 7137–7144.
- H.-B. Wang, B. P. Mudraboyina, J. Li and J. A. Wisner, *Chem. Commun.*, 2010, **46**, 7343–7345.
- I. A. Kozlov, L. E. Orgel and P. E. Nielsen, *Angew. Chem., Int. Ed.*, 2000, **39**, 4292–4295.
- H. Goto, Y. Furusho and E. Yashima, *J. Am. Chem. Soc.*, 2007, **129**, 9168–9174.
- H. Yamada, Y. Furusho and E. Yashima, *J. Am. Chem. Soc.*, 2012, **134**, 7250–7253.
- D. Haldar and C. Schmuck, *Chem. Soc. Rev.*, 2009, **38**, 363–371.
- E. Yashima, N. Ousaka, D. Taura, K. Shimomura, T. Ikai and K. Maeda, *Chem. Rev.*, 2016, **116**, 13752–13990.
- M. Liu, L. Zhang and T. Wang, *Chem. Rev.*, 2015, **115**, 7304–7397.
- Z. Lv, Z. Chen, K. Shao, G. Qing and T. Sun, *Polymers*, 2016, **8**, 310.
- G. Liu, M. G. Humphrey, C. Zhang and Y. Zhao, *Chem. Soc. Rev.*, 2023, **52**, 4443–4487.
- M. Lago-Silva, M. Fernández-Míguez, R. Rodríguez, E. Quiñoá and F. Freire, *Chem. Soc. Rev.*, 2025, **53**, 793–852.
- M. Fujiki, *J. Am. Chem. Soc.*, 2000, **122**, 3336–3343.
- K. Okoshi, S. Sakurai, S. Ohsawa, J. Kumaki and E. Yashima, *Angew. Chem., Int. Ed.*, 2006, **45**, 8173–8176.
- T. Yamada, Y. Nagata and M. Sugimoto, *Chem. Commun.*, 2010, **46**, 4914–4916.
- Y. Nagata, T. Yamada, T. Adachi, Y. Akai, T. Yamamoto and M. Sugimoto, *J. Am. Chem. Soc.*, 2013, **135**, 10104–10113.
- R. M. Meudtner and S. Hecht, *Angew. Chem., Int. Ed.*, 2008, **47**, 4926–4930.
- J.-M. Suk, V. R. Naidu, X. Liu, M. S. Lah and K.-S. Jeong, *J. Am. Chem. Soc.*, 2011, **133**, 13938–13941.
- R. Katoono, S. Kawai, K. Fujiwara and T. Suzuki, *Chem. Sci.*, 2015, **6**, 6592–6600.
- D. Zhao, T. van Leeuwen, J. Cheng and B. L. Feringa, *Nat. Chem.*, 2017, **9**, 250–256.
- Y. Aidibi, S. Azar, L. Hardoin, M. Voltz, S. Goeb, M. Allain, M. Sallé, R. Costil, D. Jacquemin, B. Feringa and D. Canevet, *Angew. Chem., Int. Ed.*, 2025, **64**, e202413629.
- K. Tateno, K. Ono and H. Kawai, *Chem. – Eur. J.*, 2019, **25**, 15765–15771.
- K. Matsumura, K. Tateno, Y. Tsuchido and H. Kawai, *Chem-PlusChem*, 2021, **86**, 1421–1425.
- K. Matsumura, K. Kinjo, K. Tateno, K. Ono, Y. Tsuchido and H. Kawai, *J. Am. Chem. Soc.*, 2024, **146**, 21078–21088.
- K. Matsumura, M. Hasegawa, Y. Tsuchido and H. Kawai, *Asian J. Org. Chem.*, 2025, **14**, e202500409.
- K. Matsumura, D. Tauchi, M. Hasegawa, Y. Tsuchido and H. Kawai, *JACS Au*, 2026, **6**, 1299–1307.
- T. Otani, T. Saito, R. Sakamoto, H. Osada, A. Hirahara, N. Furukawa, N. Kutsumura, T. Matsuo and K. Tamao, *Chem. Commun.*, 2013, **49**, 6206–6208.
- K. Tateno, R. Ogawa, R. Sakamoto, M. Tsuchiya, N. Kutsumura, T. Otani, K. Ono, H. Kawai and T. Saito, *J. Org. Chem.*, 2018, **83**, 690–702.
- ¹H NMR spectra of $[\text{Ag}(\mathbf{1b})(\mathbf{2})][\text{OTf}]$ in toluene-*d*₈ or CD_2Cl_2 were nearly identical between 1.0 and 0.10 mM (Fig. S9, S10), indicating negligible dissociation. Concentration-dependent UV-vis and CD spectra (5–100 μM) showed largely consistent chiroptical signatures with a subtle intensity increase at higher concentrations (Fig. S26).
- At 10 μM , the CD intensity of $[\text{Ag}(\mathbf{1b})(\mathbf{2})][\text{OTf}]$ was comparable to that of $[\text{Ag}(\mathbf{1b})_2][\text{OTf}]$ (Fig. S29), suggesting a counterbalance between increased double-helix population and a slight reduction in intrinsic $\Delta\epsilon$.
- In MeOH, $[\text{Ag}(\mathbf{1b})_2][\text{OTf}]$ showed a negative Cotton effect due to aggregation, whereas $[\text{Ag}(\mathbf{1b})(\mathbf{2a})][\text{OTf}]$ exhibited a positive one owing to steric suppression of aggregation.
- (a) CCDC 2534923: Experimental Crystal Structure Determination, 2026, DOI: [10.5517/ccdc.csd.cc2r2sqc](https://doi.org/10.5517/ccdc.csd.cc2r2sqc); (b) CCDC 2534924: Experimental Crystal Structure Determination, 2026, DOI: [10.5517/ccdc.csd.cc2r2srd](https://doi.org/10.5517/ccdc.csd.cc2r2srd).

